Available online at www.sciencedirect.com

ScienceDirect

Advances in Space Research 74 (2024) 3496–3510

ADVANCES IN SPACE RESEARCH (a COSPAR publication)

www.elsevier.com/locate/asr

Wavelet-based correlations of the global magnetic field in connection to strongest earthquakes

Alexey Lyubushin [a,*], Eugeny Rodionov [a,b]

[a] Institute of Physics of the Earth RAS, Moscow, Russia
[b] Russian State Geological Prospecting University, Moscow, Russia

Received 30 April 2024; received in revised form 1 June 2024; accepted 18 June 2024
Available online 22 June 2024

Abstract

We consider 3-component records of the magnetic field strength with a time step of 1 min at 153 stations of the INTERMAGNET network for 31 years, 1991–2021. Data analysis is based on the calculation of pairwise correlation coefficients between wavelet coefficients in successive time windows 1 day long (1440 min counts). To describe the state of the magnetic field, the maxima of the average values of all pairwise correlation coefficients between stations were chosen, calculated over all detail levels of the wavelet decomposition and over all components of the magnetic field strength vector. The daily time series of such maxima is called wavelet correlation. The division of the network stations into 7 clusters is considered, and a time series of wavelet correlations is calculated for each cluster. In a sliding time window with a length of 365 days, correlation measures of synchronization of wavelet correlations from different clusters are calculated, which are compared with the strongest earthquakes with a magnitude of at least 8.5. For the global time series of wavelet correlations, the method of influence matrices is used to study the relationship between the maximum correlation responses to a change in the length of the day and a sequence of earthquakes with a magnitude of at least 7. As a result of the analysis, precursor effects are identified, and the important role of the Maule earthquake in Chile on February 27, 2010 in the behavior of the response of magnetic field for the preparation of strong seismic events is shown.

Keywords: Earth's magnetic field; Seismic events; Wavelets; Correlation; Interacting point processes; Irregularity of the Earth's rotation

1. Introduction

Research into the connections between the magnetic field and the seismic process is a traditional research topic. In the (Chen et al., 2022; Jin et al., 2015) an overview of studies regarding the connections between seismic and electromagnetic phenomena and about connection of the total electron content in the ionosphere with precursor and post-seismic anomalies in connection with major earthquakes using records from global navigation satellite systems are presented. Electromagnetic precursors and changes of the structure of natural low-frequency radio noise near earthquake epicenters were studied in (Sarkar et al., 2007; Thomas et al., 2009; Xu et al., 2013; Harrison et al., 2010). Induced currents in the Earth's lithosphere in connection to field of tectonic stresses and seismic activity were investigated in (Duma and Ruzhin, 2003; Rabeh et al., 2010). Methods for extracting anomalous behavior and strong pulsed disturbances before earthquakes in electromagnetic time series are presented in (Kappler et al., 2019; Freund et al., 2021). Multidimensional methods of principal components and singular spectrum analysis for

* Corresponding author.
E-mail addresses: lyubushin@yandex.ru (A. Lyubushin), evgeny_980@list.ru (E. Rodionov).

https://doi.org/10.1016/j.asr.2024.06.046

processing time series of electromagnetic field variations were used in (Serita et al., 2005). The statistical studies of a trigger effects from the influence of the Sun on the Earth in the occurrence of earthquakes were carried out in (Love and Thomas, 2013). Origin of electric and magnetic precursors before strong earthquakes was investigated in (Varotsos et al., 2003). Natural time technique for electromagnetic data analysis with a purpose extracting precursory effects was used in (Varotsos et al., 2024).

Data from long-term monitoring of the Earth's magnetic field strength at INTERMAGNET network stations make it possible to study the statistical properties of the Earth's electromagnetic background (Matzka et al., 2010). This article proposes a statistical method for analyzing magnetic field fluctuation data from the global network of INTERMAGNET stations, based on the use of their spatial and temporal correlations, assessed using wavelet analysis for the time interval 1991–2021. Previously, a similar approach for analyzing long-term continuous records of global and regional seismic noise was used in (Lyubushin, 2018, 2020c, 2021(a,b), 2022, 2023), which mainly used a spectral approach. But for geomagnetic data with a time step of 1 min, the orthogonal wavelet analysis used in this article is more suitable due to the presence of non-stationary high-amplitude chaotic pulsations of the time series. It is shown that bursts of global wavelet correlations occur shortly before the moments of the strongest earthquakes with a magnitude of at least 8.5. Studies focusing on the precursors of mega-earthquakes have already performed in (Sarlis et al., 2015; Christopoulos et al, 2022) by applying natural time approach.

An important component of the presented approach is the analysis of the connections between the maximum spectral responses of wavelet correlations of the magnetic field to the irregular rotation of the Earth and the sequence of earthquakes with a magnitude of at least 7. To analyze this connection, a parametric model of the intensity of interacting point processes was used.

2. Initial data

The data of 3-component measurements of the Earth's magnetic field strength at 153 stations of the INTERMAGNET network (https://intermagnet.org/) are analyzed with a time step of 1 min for observations during 31 years, 1991–2021 (Fig. 1). Next, we will analyze both all the data together and when they are divided into a certain number of clusters for subsequent analysis of the effects of synchronization of the behavior of the magnetic field within these clusters.

To divide the network of stations into clusters, 7 reference points were selected (Fig. 1). The number 7 was chosen as the optimal number of station clusters, which splits their "cloud" using the k-means method. Let us partition the set of station position vectors ζ into a given trial number q of clusters using the popular k-means clustering method (Duda et al, 2000). Denote by C_r, $r = 1, ..., q$ clusters, let $z_r = \sum_{\zeta \in C_r} \zeta / n_r$ be the center of mass vector of the cluster C_r, n_r be the number of vectors in the cluster C_r, $\sum_{r=1}^{q} n_r = N$. A vector $\zeta \in C_r$ if the distance $|\zeta - z_r|$ is minimal among the positions of all cluster centers. The k-means method minimizes the sum of distances:

$$G(z_1, ..., z_q) = \sum_{r=1}^{q} \sum_{\zeta \in C_r} |\zeta - z_r|^2 \rightarrow \min_{z_1, ..., z_q} \quad (1)$$

with respect to the position of cluster centers z_r. Let $\Phi(q) = \min_{z_1, ..., z_q} G(z_1, ..., z_q)$. We used a trial number of clusters in the range $2 \le q \le 12$. The problem of choosing the best number of clusters q^* was solved using the pseudo-F-statistic maximum criterion (Vogel and Wong, 1979)

$$PFS(q) = \sigma_1^2(q) / \sigma_0^2(q) \rightarrow \max_{2 \le q \le 12} \quad (2)$$

where

$$\sigma_0^2(q) = \frac{\Phi(q)}{N - q}, \; \sigma_1^2(q) = \sum_{r=1}^{q} \frac{n_r}{N} \cdot |z_r - z_0|^2,$$

$$z_0 = \frac{1}{N} \sum_{1}^{N} \zeta \quad (3)$$

One of the graphs in Fig. 2 presents the values of the pseudo-F-statistic as a function of the trial number of clusters. The number 7 on the graph of the pseudo-F-statistics is the breakpoint of the dependence on the trial number of clusters and realizes the maximum for the number of clusters from 2 to 12. In addition, Fig. 2 shows the graphs of the annual number of workstations in each cluster with the selected partition of all 153 stations networks.

In the next Sections 3–6 of the paper the description of the used methods will be presented before presenting the results of their applications.

3. Wavelet correlations

The purpose of the analysis is to evaluate the correlations of magnetic field variations in successive time windows of 1440 min (1 day) and to evaluate the relationship between magnetic field correlations and a sequence of strong earthquakes. The analysis is performed independently for each position of the time window. Before the wavelet decomposition of the analyzed time series fragments, which is presented in the current time window, the following sequence of operations is applied to each fragment: 1) the general linear trend within the time window is removed; 2) coming to increments is performed; 3) a tapering operation is performed after coming to increments within each time window; 4) the winsorisation operation for the level of four standard deviations to ensure the robustness of estimates.

First two operations remove the strongest low frequency variations in signals, which cannot be statistically representative within the window. Tapering is a usual preliminary

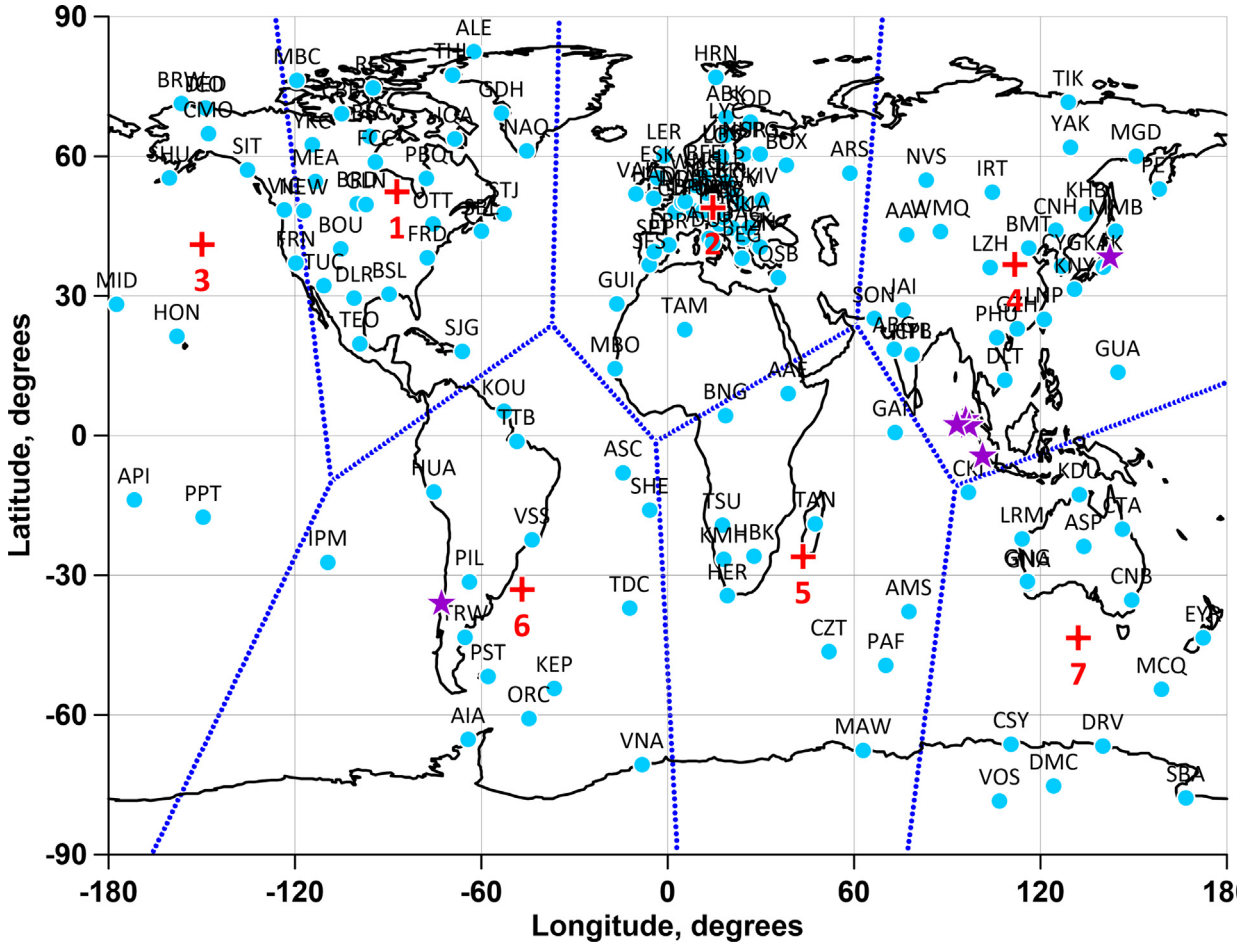

Fig. 1. The blue circles show the positions of 153 INTERMANET stations along with their identifiers. Red numbered crosses show the centers of 7 clusters of stations for which the Voronoi partition was constructed. Purple starts indicate epicenters of 6 $M \geq 8.5$ earthquakes.

operation in spectral and wavelet analysis before applying discrete Fourier or wavelet transform. It consists in multiplying the samples within current time window by the positive function, which is tending to zero, when samples approach the left and right ends of the window. We use a cosine tapering function which equals $(1-\cos(\pi t/L))/2$ for $0 \leq t \leq L$ and $(1-\cos(\pi(t-(N-1))/L))/2$ for $(N-1)-L \leq t \leq (N-1)$ where N is the length of time window in number of samples (in our case $N = 1440$). Here L is the length of time intervals at the beginning and at the end of time window, where tapering operation is performed. We used the value $L = N/8$. Tapering operation is necessary for reducing negative "wrap-around" effect of finite discrete wavelet transform (Press et al., 1996). Winsorization (Huber and Ronchetti, 2009) consists of eliminating outliers that fall outside the levels $m \pm 4\sigma$ by cutting off the time series values in each time window (m and σ are sample estimates of the mathematical expectation and standard deviation for the current time window).

To obtain correlation estimates, the Db03 orthogonal Daubechies wavelet expansion with three vanishing moments is used (Mallat, 1999). The Db03 wavelet was selected by enumeration of bases with the number of vanishing moments from 1 to 10, as realizing the minimum entropy of the distribution of squared wavelet coefficients in the largest number of cases for a sequence of intervals with a length of 1 day. The wavelet coefficients were calculated in consecutive time windows 1 day long for the first 7 levels of detail of the wavelet decomposition. The last, 7th level of detail corresponds to periods from 128 to 256 min.

At each detail level in each time window, the absolute values of the pairwise correlation coefficients between the wavelet coefficients for each pair of stations were calculated, which were then averaged. The maximum detail level of the wavelet decomposition 7 was chosen from the condition that it contains at least 8 wavelet coefficients. Then the maximum value was taken for all 7 levels of details. Further, from these maximum values calculated for the three components of the magnetic field, the maxima were selected. Let us call *wavelet correlations* the results of such sequences of maximizing operations. Wavelet correlations are time series with a time step of 1 day. According to the definition, to calculate wavelet correlations, the number of jointly processed stations must be at least 2.

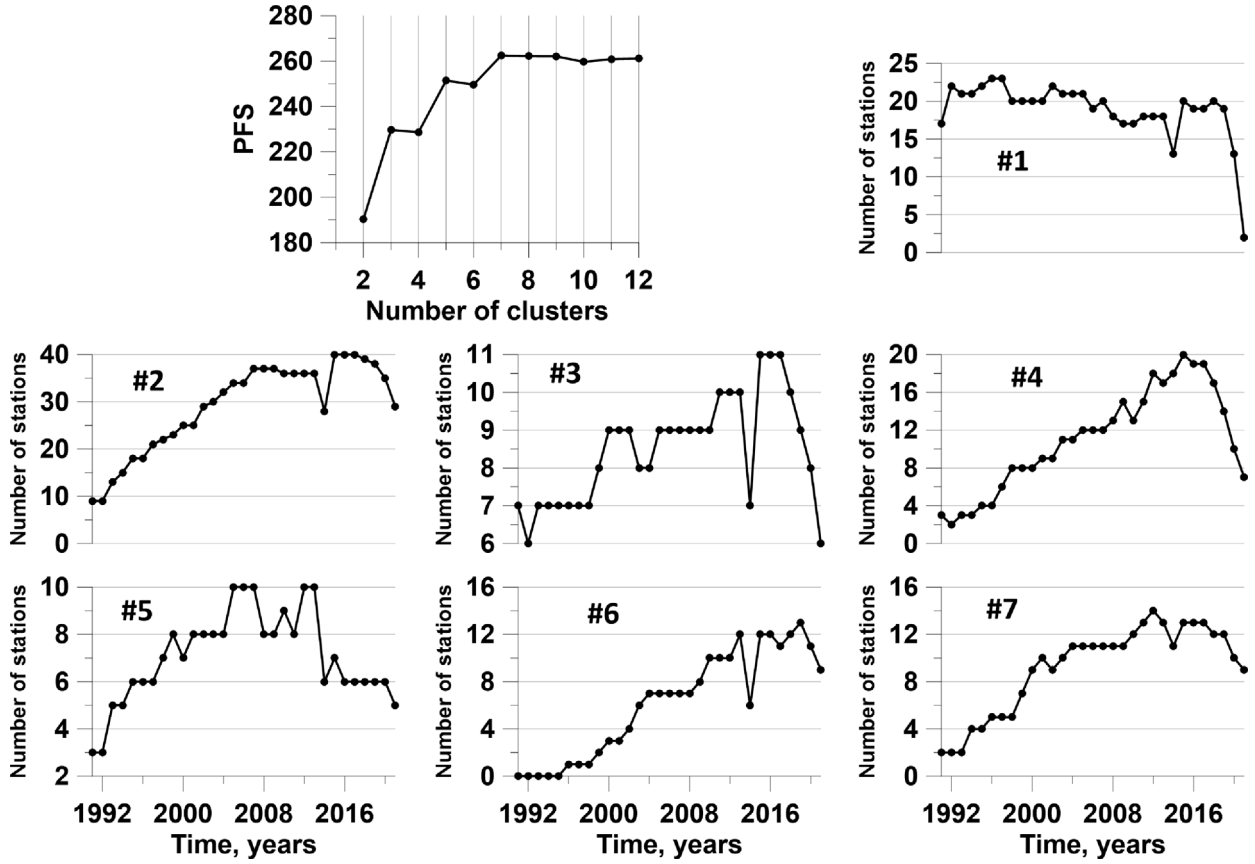

Fig. 2. A plot of the pseudo-F-statistic against the trial number of clusters is presented, which explains the choice of 7 clusters. For all clusters, graphs of the annual number of operating stations are plotted.

Fig. 3 present initial stages of calculating wavelet correlations on the example of 1440-minute fragment of the magnetic induction records at one of the station.

4. Maximum correlation matrix eigenvalue and multiple correlation coefficient

Let's denote by $Z(t)$ the $q-$dimensional time series. Denote by C_{ZZ} the correlation matrix of the time series $Z(t)$, and by μ its normalized maximum eigenvalue:

$$\mu = \lambda_1 / \sum_{k=1}^{q} \lambda_k \tag{4}$$

Within formula (4) $\lambda_1, ..., \lambda_q$ are the eigenvalues of the correlation matrix C_{ZZ}, ordered by decreasing $\lambda_k \geq \lambda_{k+1}$. According to the method of principal components (Jolliffe, 1986), the value μ is equal to the fraction of the total energy of oscillations attributable to the first principal component of the multidimensional time series and is a measure of synchronization of oscillations in scalar components of $Z(t)$. We will calculated the correlation matrix C_{ZZ} in a sliding time window. Therefore, the normalized maximum eigenvalue μ becomes a function of the position of the right end of the sliding time window.

Other way to highlight common effects in variations in multivariate time series is to use a multiple correlation coefficient (Lyubushin, 2018) based on the use of canonical correlations. We define the multiple correlation coefficient for the $q-$dimensional time series $Z(t)$ by the formula:

$$\rho = \prod_{i=1}^{q} v_i \tag{5}$$

where v_i are the square roots of the canonical quadratic correlation (Hotelling, 1936; Rao, 1965) between the $i-$th component of the vector $Z(t)$ and all other components that form the $(q-1)-$dimensional vector. The values v_i^2 are calculated by the formula (Lyubushin, 2018):

$$v_i^2 = C_i^T \left(C_{ZZ}^{(i)}\right)^{-1} C_i / P_i \tag{6}$$

Here $C_{ZZ}^{(i)}$ is a Hermitian matrix of size $(q-1) \times (q-1)$, which is obtained from the full size correlation matrix C_{ZZ} of the multivariate time series $Z(t)$ by removing the $i-$th column and $i-$th row, C_i is a $(q-1)-$dimensional vector consisting of the correlation coefficients between the $i-$th component of the vector $Z(t)$ with all its other scalar components. The quantity P_i is the variance of the $i-$th component of the vector $Z(t)$.

The value v_i^2 is a measure of the linear connectivity of the variations of the $i-$th component of the $q-$dimensional

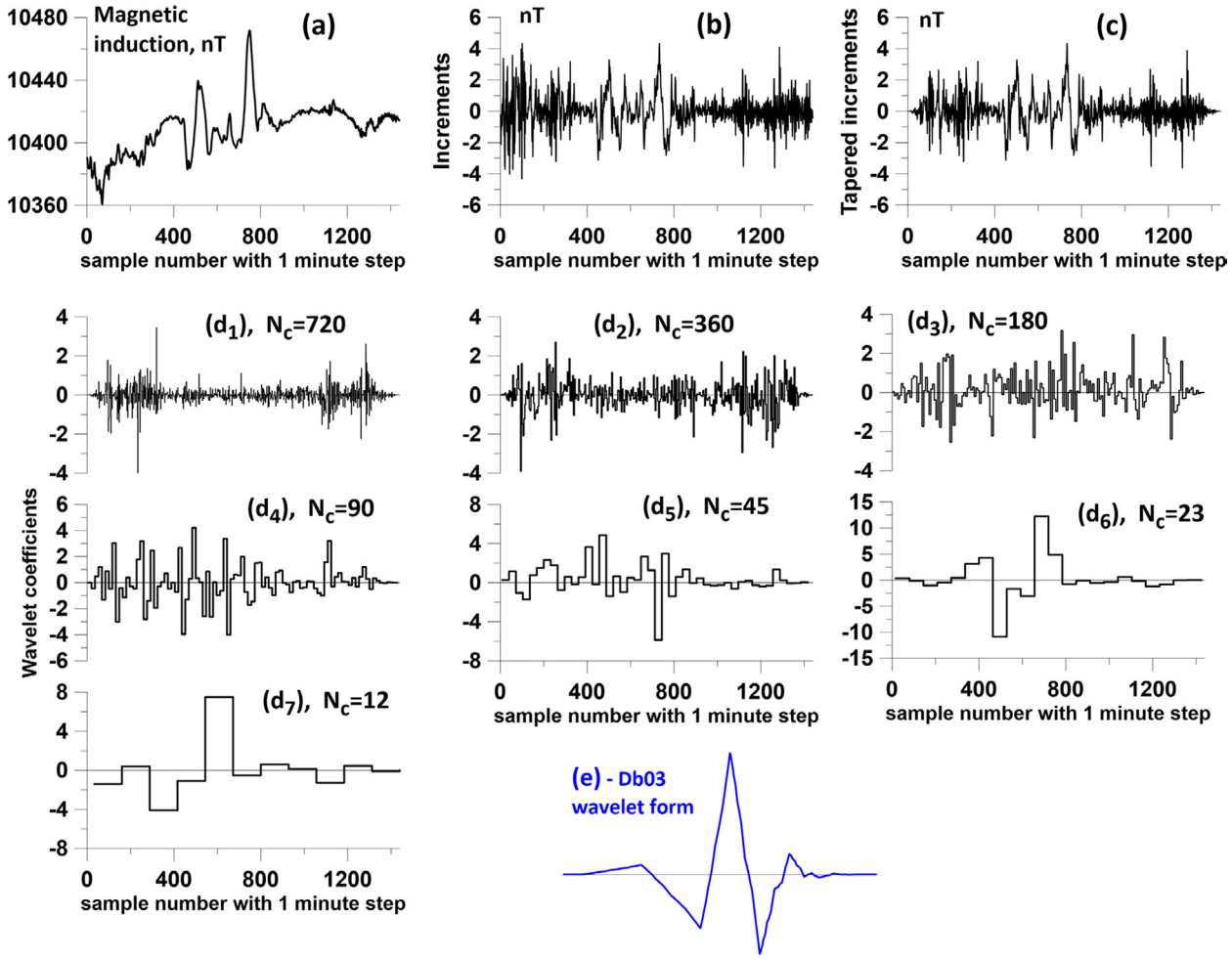

Fig. 3. Plot (a) is the graph of the daily fragment of initial INTERMAGNET record; (b) is the graph of increments; (c) is the graph of increments after tapering operation; (d_1)-(d_7) are stepwise graphs of wavelet coefficients at the detail levels 1–7; N_c is the number of wavelet coefficients at each detail level; (e) is the form of mother Db03 wavelet basis function with finite time support. Graphs (d_1)-(d_7) of wavelet coefficients were shown as stepwise in order to indicate the temporary area of responsibility of each coefficient.

vector $Z(t)$ with the variations of all other scalar components of this vector. According to the construction, the inequality $0 \le v_i \le 1$ is satisfied and the closer the value v_i is to unity, the stronger the linear relationship of the $i-$th scalar time series with all other components.

Thus, the value ρ is a "hard" measure of the linear connectivity of all components of the vector $Z(t)$ with each other, which is set to zero if at least one of the values v_i is equal to zero. The maxima of this measure highlight the strongest synchronization effects.

5. Spectral coherence

For further analysis, we will need to calculate the squared modulus of the coherence spectrum between two time series is a moving time window. A parametric model of vector autoregression which has a better frequency resolution than Fourier-based methods for estimating the spectra and cross-spectra (Marple, 1987) will be used. For a time series $X(t)$ of dimensionality q the AR-model is given by the formula:

$$X(t) + \sum_{k=1}^{p} B_k \cdot X(t-k) = \varepsilon(t) \tag{7}$$

Here t is the discrete time index, p is the order of autoregression, B_k are the matrices of autoregression coefficients of the size $q \times q$, $\varepsilon(t)$ is the residual signal covariance matrix $P = M\{\varepsilon(t)\varepsilon^T(t)\}$ of size $q \times q$. The matrices B_k and P are calculated by Durbin-Levinson procedure (Marple, 1987). The parametric estimate of spectral matrix is defined by the formula:

$$S_{XX}(\omega) = \Phi^{-1}(\omega) \cdot P \cdot \Phi^{-H}(\omega), \Phi(\omega) = E + \sum_{k=1}^{p} B_k e^{-i\omega k} \tag{8}$$

where E is the unit size $q \times q$ matrix. For dimension $q = 2$ the quadratic coherence spectrum is calculated according to formula:

$$\gamma^2(\omega) = |S_{12}(\omega)|^2 / (S_{11}(\omega) \cdot S_{22}(\omega)) \tag{9}$$

Here $S_{11}(\omega)$ and $S_{22}(\omega)$ are the diagonal elements of matrix (7) whereas $S_{12}(\omega)$ is cross-spectrum. The coherence estimation was performed using a 5th order vector autoregressive model with preliminary removal of linear trends and transition to increments.

6. Influence matrices method for two point processes

The method of influence matrices is used for investigating the relations between two sequences of events. The method was used in (Lyubushin, 2022) to analyze the relationships between local extrema of the average values of seismic noise properties and the strongest earthquakes.

Let $t_j^{(\alpha)},\ j=1,...,N_\alpha;\ \alpha=1,2$ be occurrence times of 2 sequences of events. We represent their intensities in the form:

$$\lambda^{(\alpha)}(t)=b_0^{(\alpha)}+\sum_{\beta=1}^{2}b_\beta^{(\alpha)}\cdot g^{(\beta)}(t) \tag{10}$$

where $b_0^{(\alpha)}\ge 0, b_\beta^{(\alpha)}\ge 0$ are the parameters, $g^{(\beta)}(t)$ is the function of the influence of the events $t_j^{(\beta)}$ of the sequence with the number β:

$$g^{(\beta)}(t)=\sum_{t_j^{(\beta)}<t}\exp(-(t-t_j^{(\beta)})/\tau) \tag{11}$$

According to formula (11), the weight of the event $\#j$ becomes non-zero for times $t>t_j^{(\beta)}$ and decays with the relaxation time τ. The parameter $b_\beta^{(\alpha)}$ determines the degree of influence of the sequence $\#\beta$ on the sequence $\#\alpha$. The parameter $b_\alpha^{(\alpha)}$ determines the degree of influence of the sequence $\#\alpha$ on itself (self-excitation), and the parameter $b_0^{(\alpha)}$ reflects a purely random (Poisson) intensity component. We fix the parameter τ and consider the problem of determining the parameters $b_0^{(\alpha)}, b_\beta^{(\alpha)}$. The log-likelihood for a non-stationary Poisson process over a time interval is (Cox and Lewis, 1966):

$$\ln(L_\alpha)=\sum_{j=1}^{N_\alpha}\ln(\lambda^{(\alpha)}(t_j^{(\alpha)}))-\int_0^T\lambda^{(\alpha)}(s)ds,\quad \alpha=1,2 \tag{12}$$

It is necessary to find the maximum of functions (12) with respect to the parameters. The following expression takes place:

$$b_0^{(\alpha)}\frac{\partial\ln(L_\alpha)}{\partial b_0^{(\alpha)}}+\sum_{\beta=1}^{2}b_\beta^{(\alpha)}\frac{\partial\ln(L_\alpha)}{\partial b_\beta^{(\alpha)}}=N_\alpha-\int_0^T\lambda^{(\alpha)}(s)ds \tag{13}$$

Since the parameters $b_0^{(\alpha)}, b_\beta^{(\alpha)}$ must be non-negative, then each term on the left side of this formula is equal to zero at the maximum point of function (12) – either due to the necessary conditions for the extremum (if the parameters are positive), or if the maximum is reached at the boundary, then the parameters themselves are equal to zero. Therefore, at the maximum point of the likelihood function, the following equality holds:

$$\int_0^T\lambda^{(\alpha)}(s)ds=N_\alpha \tag{14}$$

We substitute the expression $g^{(\beta)}(t)$ from (10) into (13) and divide by T. Then we get another form of formula (14):

$$b_0^{(\alpha)}+\sum_{\beta=1}^{m}b_\beta^{(\alpha)}\cdot\bar{g}^{(\beta)}=\lambda_0^{(\alpha)}\equiv N_\alpha/T \tag{15}$$

where

$$\bar{g}^{(\beta)}=\int_0^T g^{(\beta)}(s)ds/T \tag{16}$$

– the mean value of the influence function. Substituting $b_0^{(\alpha)}$ from (15) into (12), we obtain the next maximum problem:

$$\Phi^{(\alpha)}(b_1^{(\alpha)},b_2^{(\alpha)})=\sum_{j=1}^{N_\alpha}\ln(\lambda_0^{(\alpha)}+\sum_{\beta=1}^{2}b_\beta^{(\alpha)}\cdot\Delta g^{(\beta)}(t_j^{(\alpha)}))\to\max \tag{17}$$

where $\Delta g^{(\beta)}(t)=g^{(\beta)}(t)-\bar{g}^{(\beta)}$, under restrictions:

$$b_1^{(\alpha)}\ge 0, b_2^{(\alpha)}\ge 0, \sum_{\beta=1}^{2}b_\beta^{(\alpha)}\bar{g}^{(\beta)}\le\lambda_0^{(\alpha)} \tag{18}$$

Function (17) is convex with a negative definite Hessian and, therefore, problem (17–18) has a unique solution. Having solved numerically the problem (17–18) for a given τ, you can enter the elements of the influence matrix $\kappa_\beta^{(\alpha)}, \alpha=1,2;\ \beta=0,1,2$ according to the formulas:

$$\kappa_0^{(\alpha)}=\frac{b_0^{(\alpha)}}{\lambda_0^{(\alpha)}}\ge 0,\quad \kappa_\beta^{(\alpha)}=\frac{b_\beta^{(\alpha)}\cdot\bar{g}^{(\beta)}}{\lambda_0^{(\alpha)}}\ge 0 \tag{19}$$

The value $\kappa_0^{(\alpha)}$ is share of the mean intensity $\lambda_0^{(\alpha)}$ of the process $\#\alpha$, which is purely stochastic, the share $\kappa_\alpha^{(\alpha)}$ is caused by the influence of self-excitation $\alpha\to\alpha$ and $\kappa_\beta^{(\alpha)},\ \beta\ne\alpha$ is due to external influence $\beta\to\alpha$. Formula (15) implies the normalization condition:

$$\kappa_0^{(\alpha)}+\sum_{\beta=1}^{2}\kappa_\beta^{(\alpha)}=1,\quad \alpha=1,2 \tag{20}$$

As a result, we can determine the influence matrix:

$$\left(\begin{array}{c|c|c}\kappa_0^{(1)} & \kappa_1^{(1)} & \kappa_2^{(1)}\\ \kappa_0^{(2)} & \kappa_1^{(2)} & \kappa_2^{(2)}\end{array}\right) \tag{21}$$

The first column of matrix (21) is composed of the Poisson shares of the average intensities. The diagonal elements of the right submatrix of size 2×2 consist of self-excited elements of medium intensity, while the off-diagonal elements correspond to mutual excitation. The sums of the constituent rows of the influence matrix (20) are equal to 1. Further the influence matrices (21) will be estimated in a

moving time window of certain length with a given value of the relaxation parameter τ.

7. Secondary correlations and their relationship with strong earthquakes

The purpose of INTERMAGNET data processing is to analyze secondary correlations, that is, correlations between daily wavelet correlations. Estimates of secondary correlations will be made in a time window of 365 days, that is, one year. In particular, we will be interested in the question of how the secondary correlations of the Earth's magnetic field are related to the strongest earthquakes.

Fig. 4 shows graphs of daily wavelet correlations for stations from 7 clusters indicated in Fig. 1. Since the number of stations in cluster #6 becomes at least 2 only in 2000, the length of the time series of wavelet correlations for this cluster is less than for other clusters and occupies the time interval 2000–2021. The green lines present smoothing by moving average in the window of the length 57 days. The purpose of this smoothing is a more comfort visual presentation of strongly chaotic variations of wavelet correlations. The length 57 days was chosen as a double length of Moon month (28 days).

We identified 6 strongest earthquakes with magnitudes not lower than 8.5: 2004.12.26, Sumatra M = 9.1; 2005.03.28, Sumatra M = 8.6; 2007.09.12, Sumatra

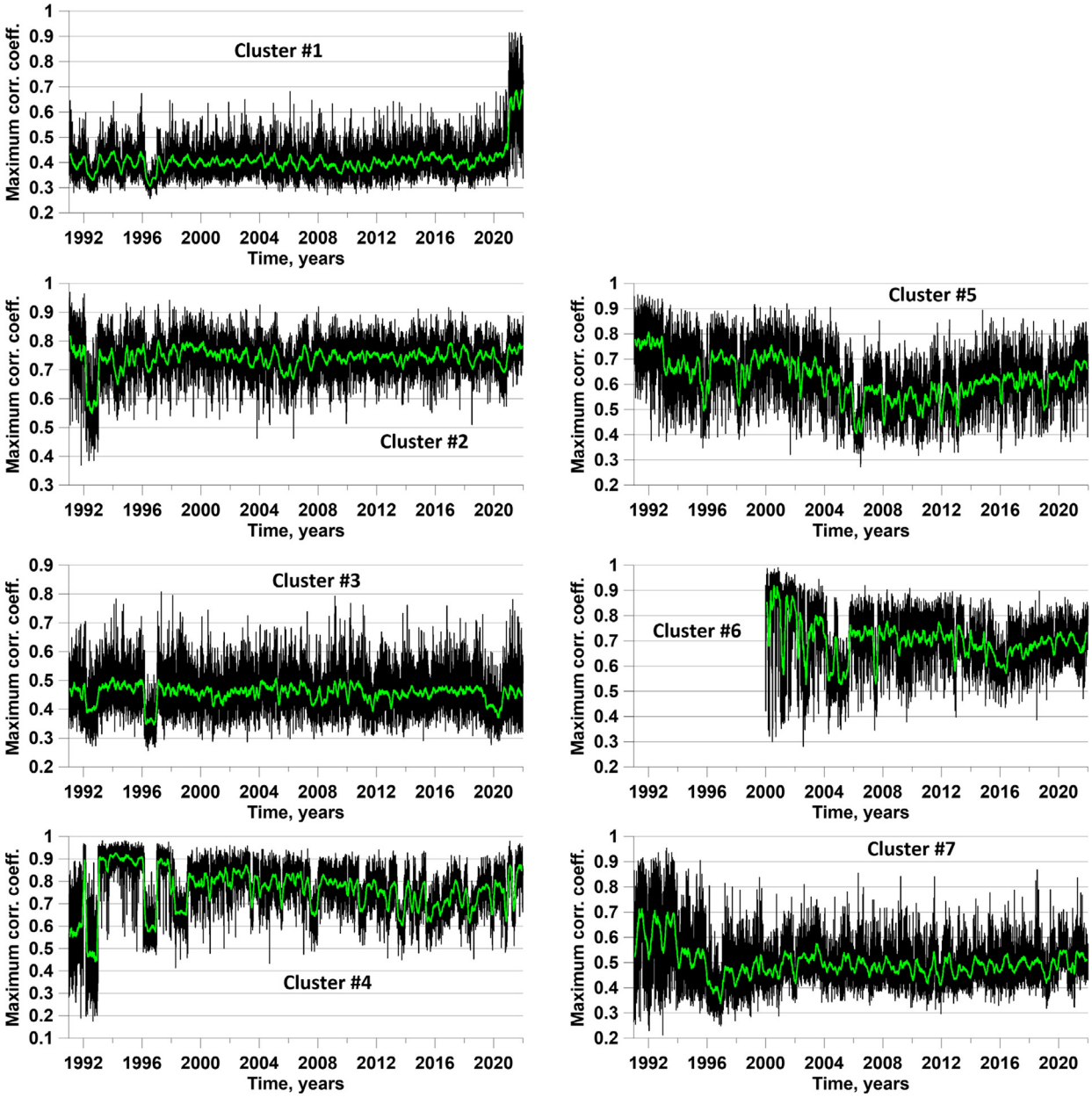

Fig. 4. Daily wavelet correlations for the results of observations of the Earth's magnetic field for stations from 7 clusters are presented. The green lines represent moving average in a 57-day window. The time series of wavelet correlations for cluster #6 can only be determined starting from the year 2000, since earlier the number of working stations for this cluster was zero.

M = 8.5; 2010.02.27, Chile (Maule), M = 8.8; 2011.03.11, Japan (Tohoku), M = 9.0; 2012.04.11, Sumatra M = 8.6.

We calculated the correlation matrix C_{ZZ} in a sliding time window of 365 days with a shift of 3 days. Before calculating the secondary correlations from the wavelet correlations in each 365-day window, the linear trend was removed, the transition to increments was carried out, and the previously mentioned winsorisation operation was performed to ensure the stability of the estimates of the correlation coefficients with respect to large outliers. Therefore, the normalized maximum eigenvalue (4) becomes a function of the position of the right end of the sliding time window. These dependencies are shown on the graphs in Fig. 5 for 2 cases, when the dimension of the vector $Z(t)$ is 6 and 7. The vertical lines indicate the time points of the 6 strongest earthquakes in the world.

It can be seen from these graphs that, basically, before strong earthquakes, synchronization is observed, which reaches local maxima and then decreases. Highlighted in red is the Maule earthquake in Chile on February 27, 2010, which, from our point of view, is characterized by the greatest precursor synchronization of the components of the wavelet correlation vectors of the magnetic field.

Besides "soft" correlation measure (4) we applied a "hard" correlation measure (5) which is based on using canonical correlations. The measure (5) can also be represented as a function of the right end of the time window. Such dependencies are shown in Fig. 6.

The graphs at the Fig. 5 show that for almost all mega-earthquakes the normalized maximum eigenvalue (4) is increasing before the events, except one earthquake on 2012.04.11 near Sumatra, which finalize the burst of strongest earthquakes activity. It can be seen from the graphs in Fig. 6 that the Maule earthquake is the time point of the strongest maximum of the measure (5), and the increase in this synchronization measure occurs approximately during the year before the event.

8. Relationship between global wavelet correlations of the magnetic field, irregularity of the Earth's rotation and the strongest earthquakes

If wavelet correlations are calculated for all stations, then the result will be a time series of global magnetic field correlations, the plot of which is shown in Fig. 7.

Further, as an "external influence" on the Earth's magnetic field, it is proposed to consider such an indicator of the unevenness of the Earth's rotation as the length of the day (LOD – length of day). Some researchers have pointed to a connection between the irregular rotation of

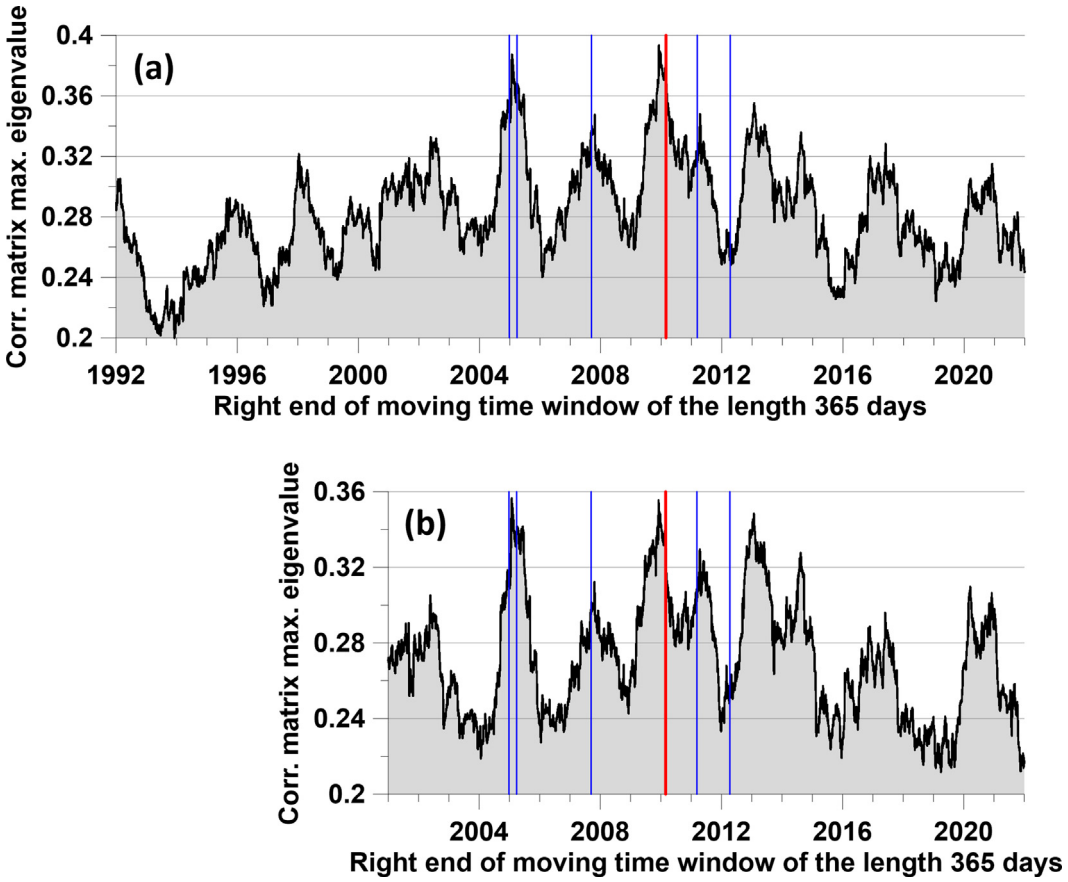

Fig. 5. (a) – plot of the maximum normalized eigenvalue of the correlation matrix of the 6-dimensional time series of wavelet correlations for clusters #1–5 and #7 in a time window of 365 days; (b) – plot of the eigenvalue of the correlation matrix of the 7-dimensional time series for all clusters #1–7. The vertical lines mark the time points of the 6 largest earthquakes with a magnitude of at least 8.5, of which the red line marks the time point of the Maule earthquake in Chile on February 27, 2010, M = 8.8.

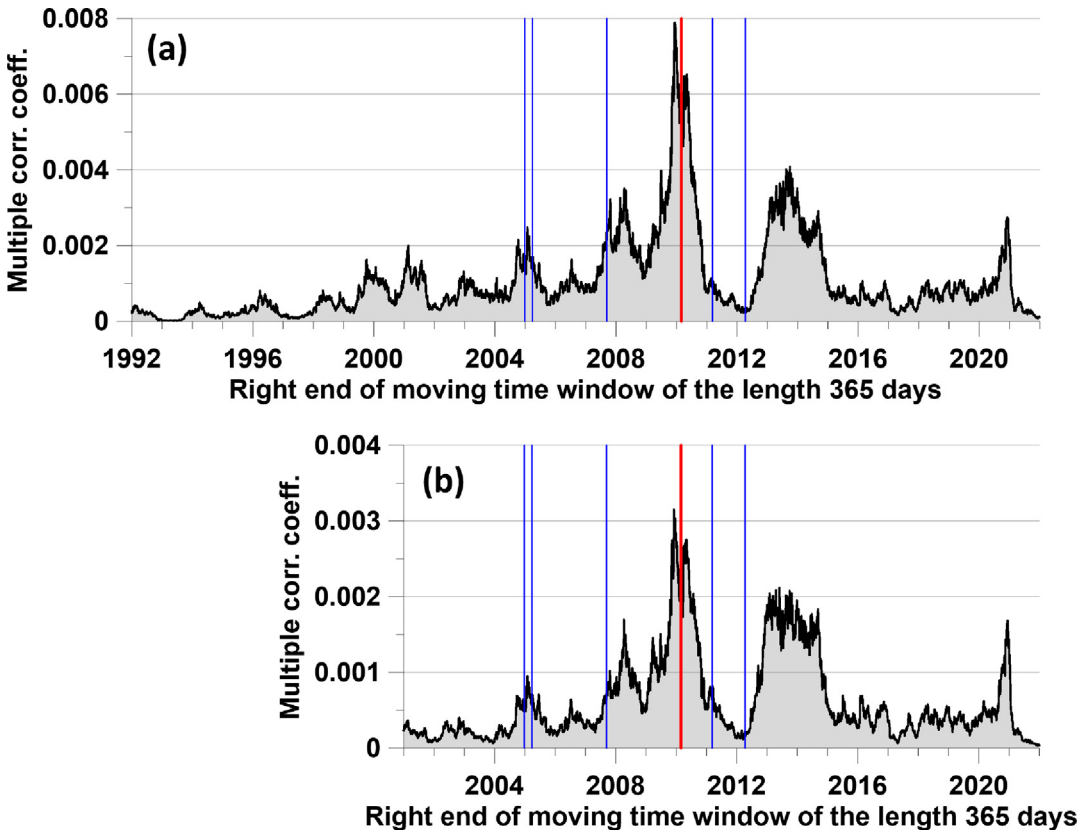

Fig. 6. (a) – plot of the multiple correlation coefficient of the 6-dimensional time series of wavelet correlations for clusters #1–5 and #7 in a time window of 365 days; (b) – plot of the multiple correlation coefficient of the 7-dimensional time series for all clusters #1–7. The vertical lines mark the time points of the 6 largest earthquakes with a magnitude of at least 8.5, of which the red line marks the time point of the Maule earthquake in Chile on February 27, 2010, M = 8.8.

the Earth and seismicity (Shanker et al, 2001). The irregularity of the Earth's rotation attracts the attention of researchers as an important factor influencing processes in the Earth's crust. In (Bendick, and Bilham, 2017), the question was investigated that rotational unevenness can be a trigger for seismic events. The work (Xu and Wenke, 2012) presents estimates of the inverse effect of a strong earthquake on the length of the day. In (Lyubushin, 2020a, 2020b, 2020c, 2021a, 2021b, 2022, 2023), the response of seismic noise properties to changes in the length of the day and the relation of this response to the probability of occurrence of strong earthquakes were studied. Next, we will also try to evaluate the influence of the irregularity of the Earth's rotation on the magnetic field correlations and find out how the response of correlations to the length of the day can be related to the probability of strong earthquakes.

The LOD time series is available from the International Earth rotation and Reference systems Service (IERS) website at https://hpiers.obspm.fr/iers/eop/eopc04/eopc04.1962-now. Further, we will use the concept of "response to LOD", in our case, the daily global wavelet correlation, the graph of which is shown in Fig. 7. The response is understood as the maximum quadratic coherence (9) between the length of the day (irregularity of the Earth's rotation) and daily wavelet correlations (Fig. 7), calculated in a sliding time window 365 days long with a shift of 3 days using a 5th order autoregressive model (7). Previously, such LOD response statistics were used in the analysis of the properties of low-frequency seismic noise in (Lyubushin, 2020a, 2020b, 2020c, 2021a, 2021b, 2022, 2023), in which the method for calculating the LOD response is described in detail.

The purpose of further analysis is to study the relationship between the response of the global wavelet correlations of the magnetic field to the irregularity of the Earth's rotation and the sequence of earthquakes with a magnitude of at least 7. The time points of 467 earthquakes with a magnitude of at least 7 and the time points of reaching the 467 largest local maxima of the response to LOD are compared. Graphs of these time series are presented in Fig. 8.

The connection between two sequences of events, which are presented at Fig. 8(b) and Fig. 8(c) will be investigated using influence matrix method which is described if Section 6 of the paper. The calculations of matrix (21) were carried out for 100 time window lengths in the range from 3 to 7 years with a shift of 0.05 years for a relaxation time τ of 0.25 years. For each length of the time window, we select the moments of time corresponding to the local maxima of

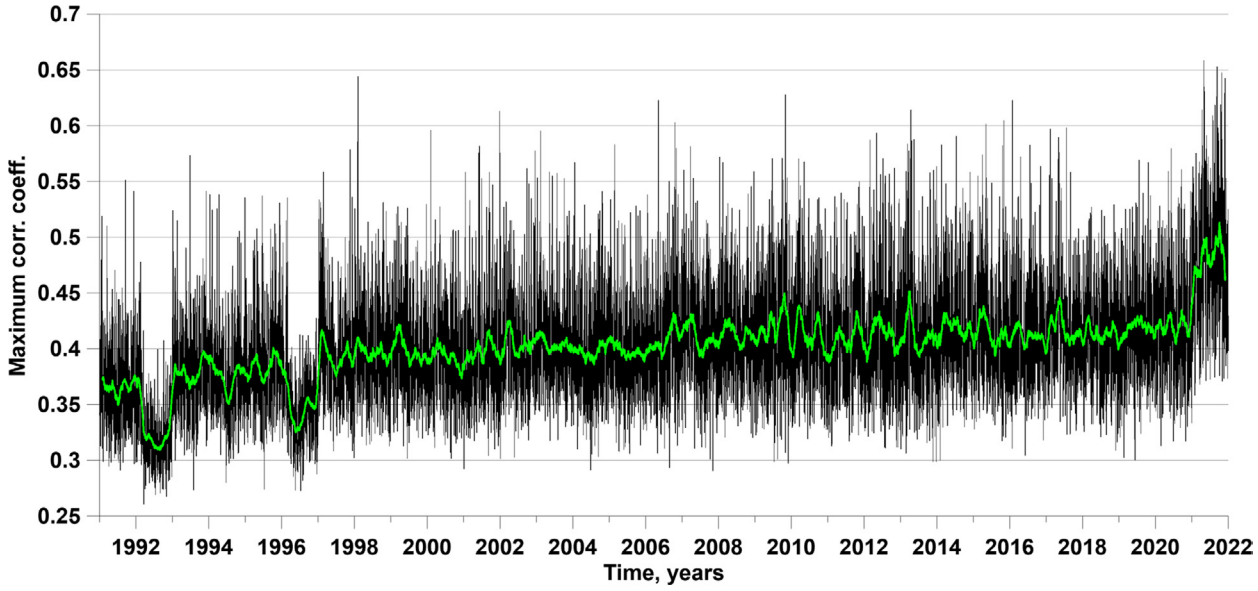

Fig. 7. Graph of daily wavelet correlations for the results of observations of the Earth's magnetic field for all stations. The green line represents the moving average in a 57-day window.

the component of the influence matrix (one of the off-diagonal elements of the right submatrix of size 2×2 in matrix (21)), corresponding to the influence of the responses of global wavelet correlations on the length of the day on the times of earthquakes when the time window is shifted along the time axis. Fig. 9 shows an example of selecting the 16 largest local maxima when assessed in a time window of 4 years.

Going through all the lengths of time windows within the given limits, we select a given number of the largest local maxima. Thus, an ensemble of estimates of influence matrices is used. The result is shown in Fig. 10 for two choices of local maxima: (a) using the 4 largest local maxima in each time window and (b) using the 32 largest local maxima.

Fig. 11 shows the numbers of the largest local maxima within "short" time intervals of 0.05 years for all time windows. These dependencies are a kind of densities of distribution of time moments of given numbers of the largest local maxima of the influence matrix component. It can

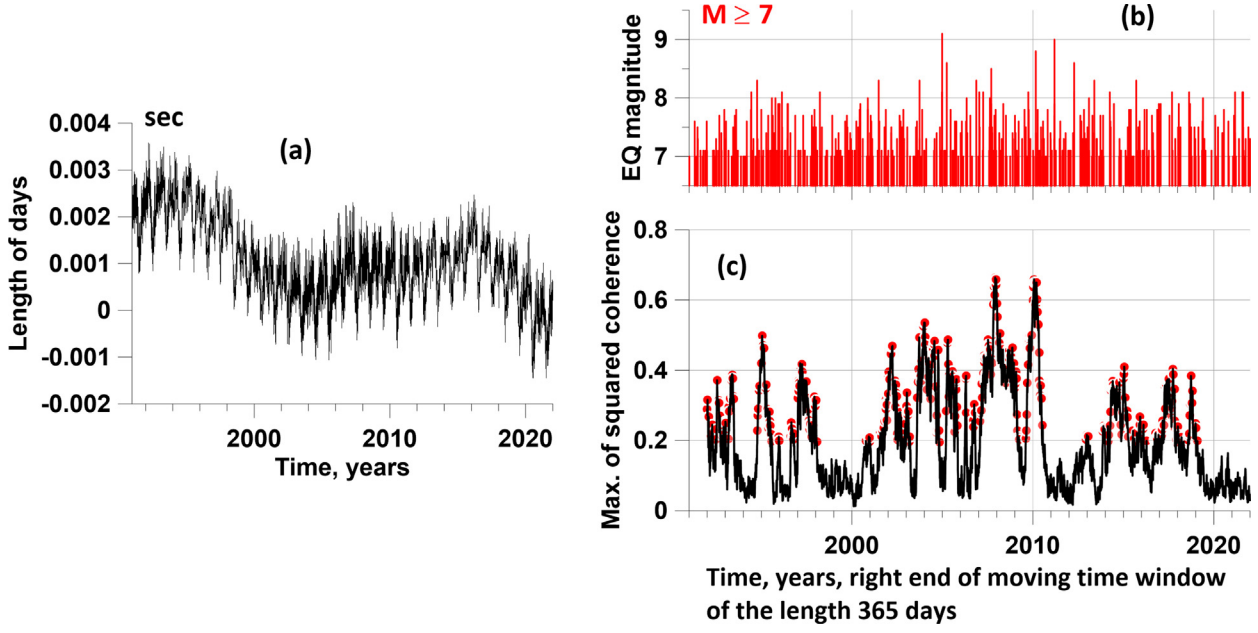

Fig. 8. (a) – plot of length of day; (b) – sequence of 467 earthquakes with a magnitude of at least 7 for the time interval 1991–2022 (https://earthquake.usgs.gov/earthquakes/search/); (c) is the response of the maximum wavelet correlations of the magnetic field to the irregularity of the Earth's rotation, the red dots mark the time points of 467 of the largest local response maxima depending on the right end of the time window.

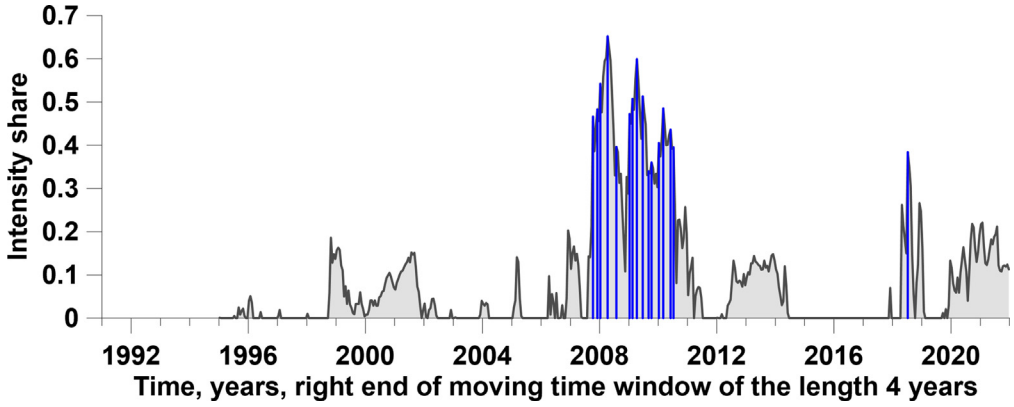

Fig. 9. The gray line shows the graph of the component of the influence matrix corresponding to the "influence" of the 467 time points of the largest local maxima of the response of the wavelet correlations of the magnetic field to the irregularity of the rotation of the Earth on a sequence of seismic events with a magnitude of at least 7; the vertical blue lines represent the times and values of the 16 largest local response maxima. The graphs are constructed for evaluation in a sliding time window of 4 years with a shift of 0.05 years for a relaxation time of 0.25 years.

be seen from the graphs in Fig. 11 that the time moments of local maxima are concentrated in the time intervals preceding the 2nd earthquakes – Maule on February 27, 2010 and Tohoku on March 11, 2011. It is interesting to note that with a large number of 32 largest local maxima, an interval of their concentration also appears at the end of the entire data processing interval. But at the same time, the amplitude of these local maxima is significantly less than before the Maule earthquake.

Let us evaluate the responses of maximum wavelet correlations to the irregular rotation of the Earth separately for each of the 6 clusters of stations that have a full implementation length of 1991–2021, that is, for all clusters, with the exception of cluster #6. Similar to previous estimates for the response to maximum wavelet correlations for all stations, we will calculate the responses in a sliding time window of 365 days with an offset of 3 days. For each response curve, we determine 467 largest local maxima, which is equal to the number of earthquakes with a magnitude of at least 7. The results of these estimates are presented in Fig. 12.

Next, for each pair of sequences of events – time points of local maxima for 6 clusters, represented in Fig. 12 by red dots, and for time points of seismic events in Fig. 8(b), we will carry out the same analysis using the method of influence matrices, which was previously done for one pair of events shown in Fig. 8(b,c). This time we will limit ourselves to graphs of the numbers of the largest local maxima for 32 maxima, which is similar to Fig. 11(d). The results of such estimates are shown in the graphs in Fig. 13.

From the graphs in Fig. 13 it is clear that for almost all clusters the predominant concentration of the maximum values of the corresponding elements of the influence matrices in the vicinity of the times of mega-earthquakes has been preserved, with the exception of cluster No. 5. Moreover, the predictive nature of the concentration of maximum values of the elements of the influence matrices is especially clearly visible for clusters 1, 2, 4 and 7. However, the result of the analysis of maximum wavelet correlations for the entire set of stations in Fig. 11 is more preferable.

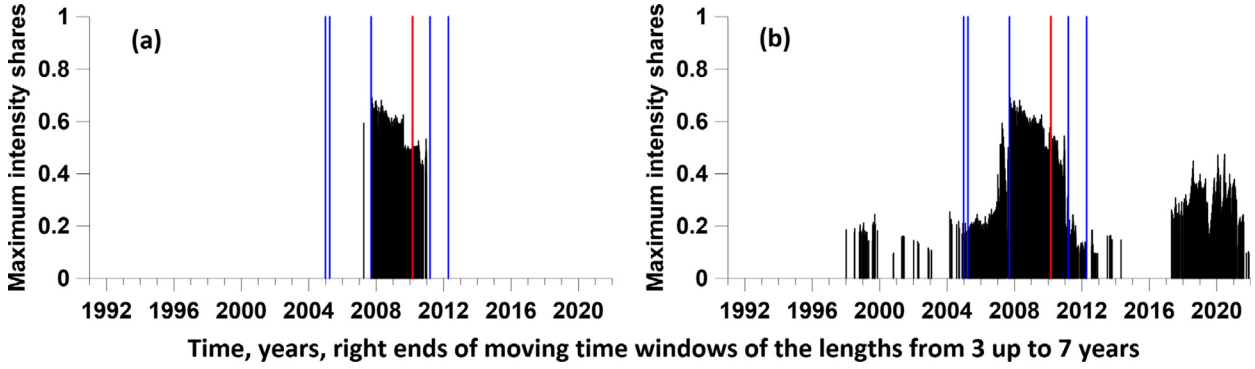

Fig. 10. Moments and magnitudes of local maxima of influence matrices in sliding time windows from 3 to 7 years long with a shift of 0.05 years, relaxation time 0.25 years; plot (a) corresponds to the use of the 4 largest local maxima of the component of the influence matrices, plot (b) corresponds to the use of 32 maximum local maxima in each time window. The vertical lines mark the time points of the 6 largest earthquakes with a magnitude of at least 8.5, of which the red line marks the time point of the Maule earthquake in Chile on February 27, 2010, M = 8.8.

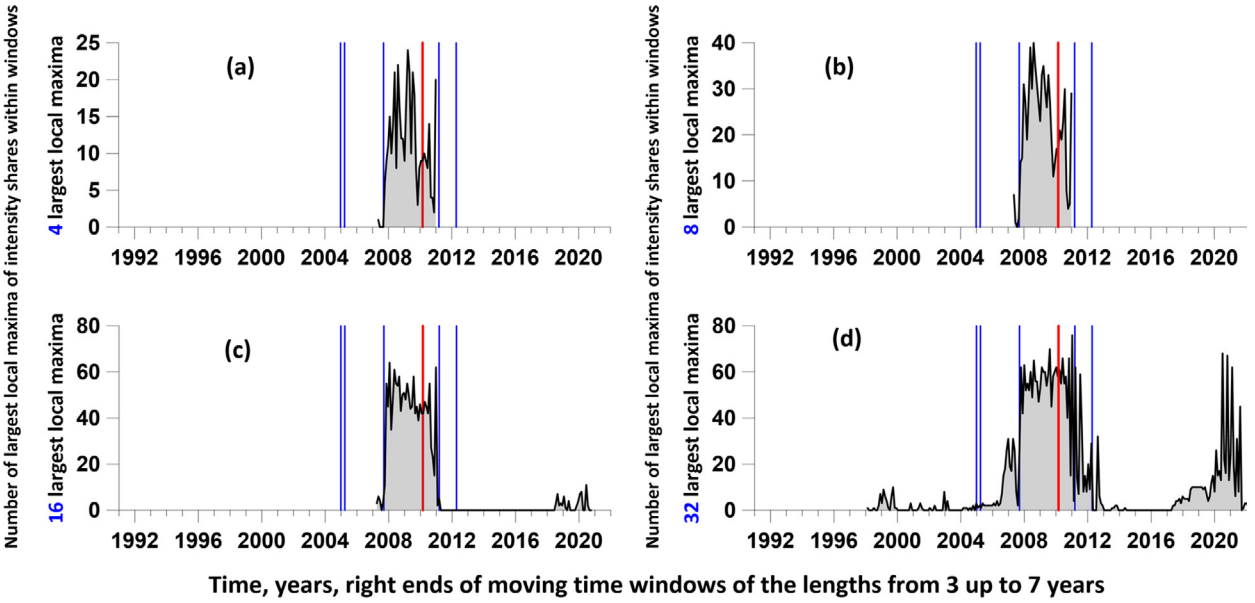

Fig. 11. (a, b, c, d) are the numbers of the largest local maxima in successive short time intervals 0.05 years long, respectively, for 4, 8, 16, and 32 largest local maxima for all time windows. The vertical lines mark the time points of the 6 largest earthquakes with a magnitude of at least 8.5, of which the red line marks the time point of the Maule earthquake in Chile on February 27, 2010, M = 8.8.

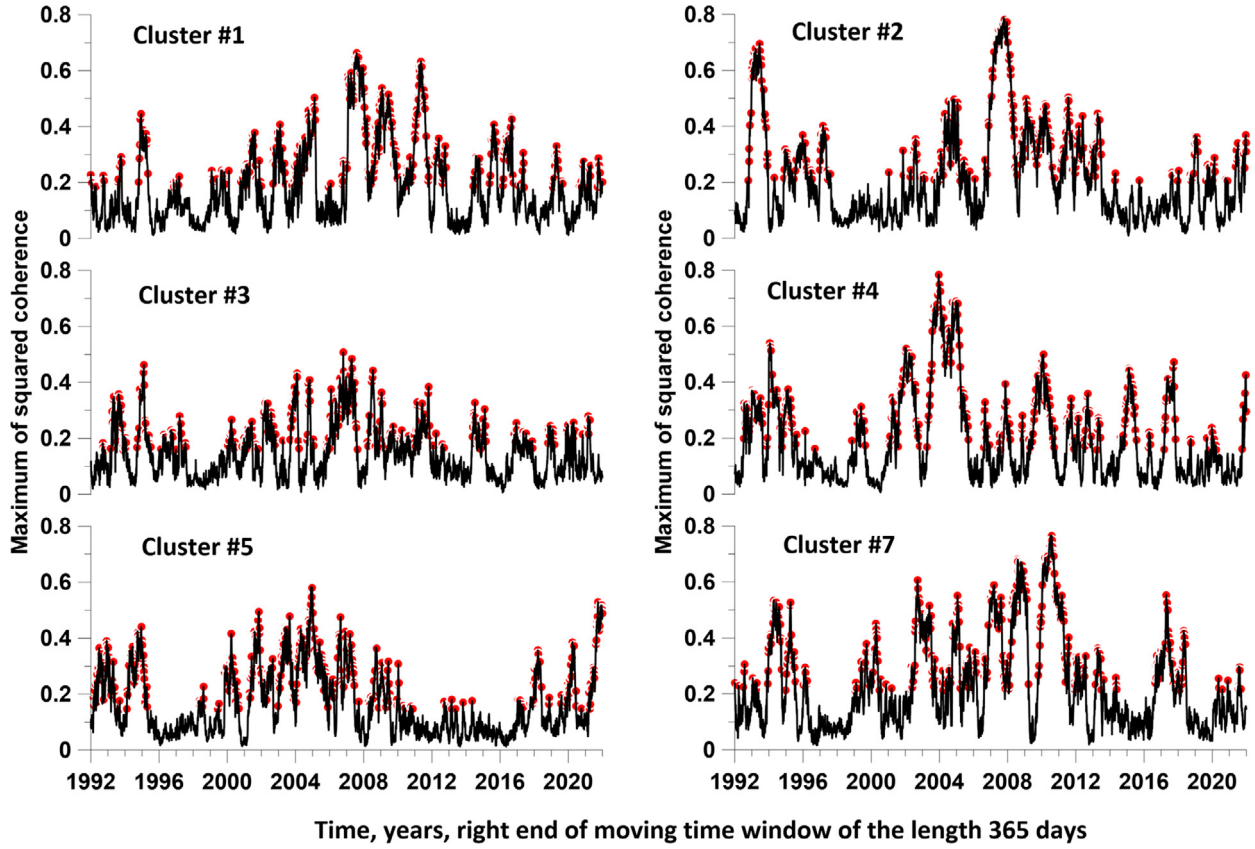

Fig. 12. Responses of the maximum wavelet correlations of the magnetic field for 6 clusters of stations to the irregularity of the Earth's rotation, the red dots mark the time points of 467 of the largest local response maxima depending on the right end of the time window of the length 365 days with mutual shift 3 days.

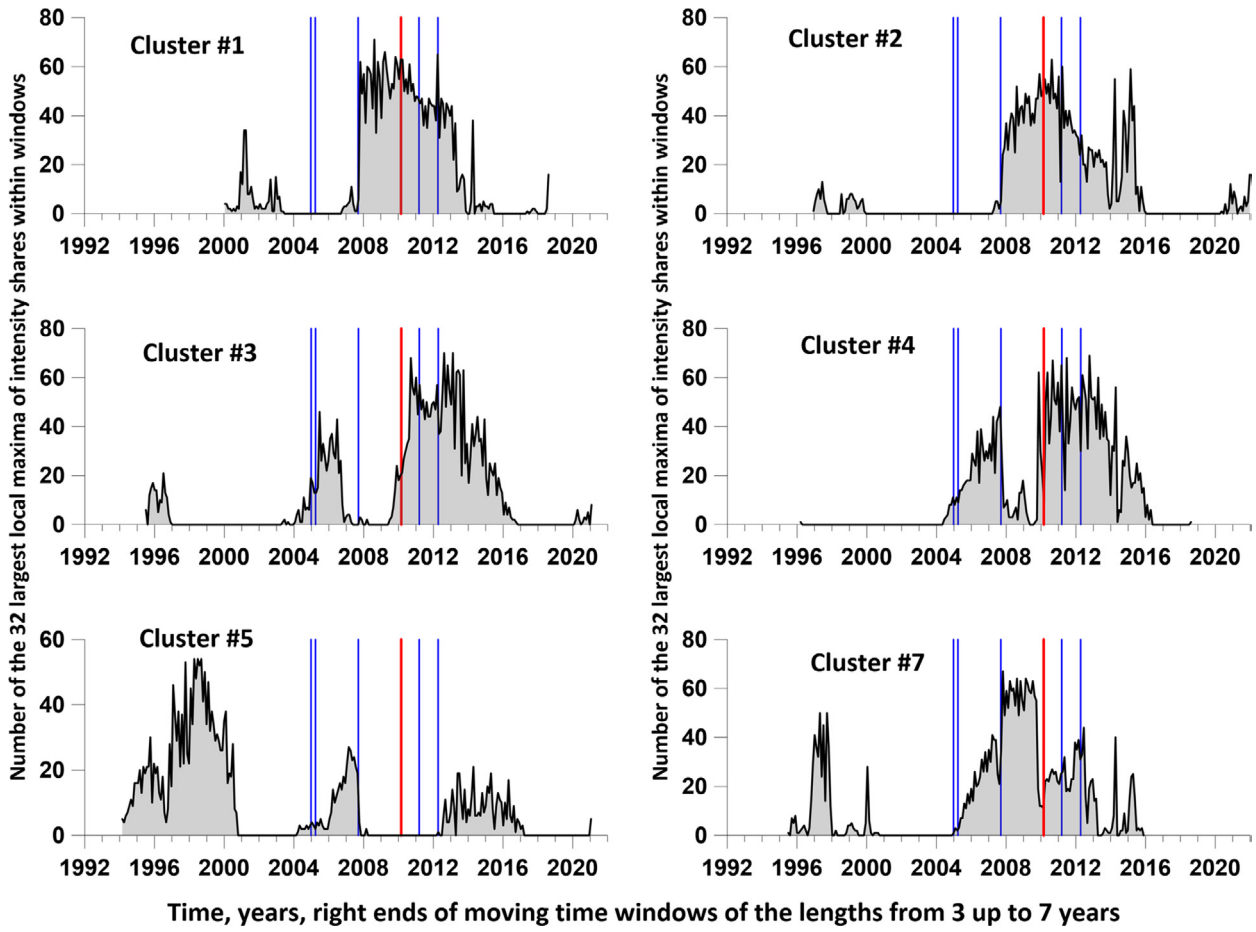

Fig. 13. Plots the numbers of the largest local maxima in successive short time intervals 0.05 years long, for 32 largest local maxima for all time windows with length from 3 up to 7 years for 6 clusters of stations. The vertical lines mark the time points of the 6 largest earthquakes with a magnitude of at least 8.5, of which the red line marks the time point of the Maule earthquake in Chile on February 27, 2010, M = 8.8.

9. Conclusions

A method for the analysis of long time series of observations of the Earth's magnetic field with a time step of 1 min, based on the expansion in orthogonal wavelets, is proposed. The concept of daily wavelet correlations is introduced. Estimates of correlation measures of synchronization of time series of wavelet correlations from 7 clusters of stations in a sliding time window of 365 days (1 year) are obtained. According to estimates of the maximum eigenvalue of the correlation matrix, for most of the strongest earthquakes in the world, there is an increase in synchronization before the events and a subsequent decrease after it. The duration of the precursor synchronization is approximately 1 year. The multiple correlation coefficient based on the use of canonical correlations singled out the Maule earthquake in Chile on 2010.02.27 among all the strongest earthquakes in the world, as an event with the strongest predictor synchronization and correlation burst amplitude. This fact indirectly confirms the hypothesis formulated in (Lyubushin, 2020c, 2021a, 2022, 2023) that a pair of the strongest earthquakes in the world, not far apart in time from each other, Maule in Chile 2010.02.27 and Tohoku in Japan, 2011.11. 03 were events of destabilization of the behavior of the low-frequency seismic noise field. Thus, the Maule event is also most strongly reflected in the behavior of the Earth's magnetic field.

It has been established that the response of the wavelet correlations of the magnetic field to the irregularity of the Earth's rotation when estimating the influence matrices for sequences of sliding time windows with a length of 3 to 7 years coincides with the time interval of earthquakes. The bursts of the components of the influence matrices in 2018–2022 independently confirm the earlier conclusions about the increase in the current seismic hazard based on the analysis of the response of seismic noise properties to LOD (Lyubushin, 2022, 2023).

Conflicts of interest

The authors declare that the research was conducted in the absence of any commercial or financial relationships that could be construed as a potential conflict of interest.

Data Availability

The open access data from the sources:
https://intermagnet.org/,
https://hpiers.obspm.fr/iers/eop/eopc04/eopc04.1962-now
https://earthquake.usgs.gov/earthquakes/search/
were used.

Acknowledgments

The work was carried out within the framework of the state assignment of the Institute of Physics of the Earth of the Russian Academy of Sciences (topic FMWU-2022-0018). This research received no external funding.

References

Bendick, R., Bilham, R., 2017. Do weak global stresses synchronize earthquakes?. Geophys. Res. Lett. 44 8320–8327. https://doi.org/10.1002/2017GL074934.

Changy, Xu, Wenke, S., 2012. Co-seismic Earth's rotation change caused by the 2012 Sumatra earthquake. Geod. Geodyn. 3 (4), 28–31. https://doi.org/10.3724/SP.J.1246.2012.00028.

Chen, H., Han, P., Hattori, K., 2022. Recent advances and challenges in the seismo-electromagnetic study: a brief review. Remote Sens. 14, 5893. https://doi.org/10.3390/rs14225893.

Christopoulos, S.-R.-G., Varotsos, P.K., Perez-Oregon, J., Papadopoulou, K.A., Skordas, E.S., Sarlis, N.V., 2022. Natural time analysis of global seismicity. Appl. Sci. 12 (15), 7496. https://doi.org/10.3390/app12157496.

Cox, D.R., Lewis, P.A.W., 1966. The statistical analysis of series of events. Methuen, London.

Duda, R.O., Hart, P.E., Stork, D.G., 2000. Pattern Classification. Wiley-Interscience Publication, New York, Chichester, Brisbane, Singapore, Toronto.

Duma, G., Ruzhin, Y., 2003. Diurnal changes of earthquake activity and geomagnetic Sq-variations. Nat. Hazards Earth Syst. Sci. 3, 171–177. https://doi.org/10.5194/nhess-3-171-2003.

Freund, F.T., Heraud, J.A., Centa, V.A., Scoville, J., 2021. Mechanism of unipolar electromagnetic pulses emitted from the hypocenters of impending earthquakes. Eur. Phys. J. Spec. Top. 230, 47–65. https://doi.org/10.1140/epjst/e2020-000244-4.

Harrison, R.G., Aplin, K.L., Rycroft, M.J., 2010. Atmospheric electricity coupling between earthquake regions and the ionosphere. J. Atmospheric and Solar-Terrestrial Physics 72, 376–381. https://doi.org/10.1016/j.jastp.2009.12.004.

Hotelling, H., 1936. Relations between two sets of variates. Biometrika 28, 321–377. https://doi.org/10.1007/978-1-4612-4380-9_14.

Huber, P.J., Ronchetti, E.M., 2009. Robust Statistics, Second ed. John Wiley & Sons, Inc., p. 354.

Jin, Sh., Occhipinti, G., Jin, R., 2015. GNSS ionospheric seismology: Recent observation evidences and characteristics. Earth Sci. Rev. 147 (2015), 54–64. https://doi.org/10.1016/j.earscirev.2015.05.003.

Jolliffe I.T., (1986) Principal Component Analysis, 1986, Springer-Verlag. https://doi.org/10.1007/b98835.

Kappler, K.N., Schneider, D.D., MacLean, L.S., Bleier, T.E., Lemon, J.J., 2019. An algorithmic framework for investigating the temporal relationship of magnetic field pulses and earthquakes applied to California. Computers and Geosci. 133104317. https://doi.org/10.1016/j.cageo.2019.104317.

Love, J.J., Thomas, J.N., 2013. Insignificant solar-terrestrial triggering of earthquakes. Geophys Res. Lett. 40, 1165–1170. https://doi.org/10.1002/grl.50211.

Lyubushin, A., 2020a. Connection of Seismic Noise Properties in Japan and California with Irregularity of Earth's Rotation. Pure Appl. Geophys. 177 (2020), 4677–4689. https://doi.org/10.1007/s00024-020-02526-9.

Lyubushin, A., 2020b. Trends of global seismic noise properties in connection to irregularity of Earth's rotation. Pure Appl. Geophys. 177, 621–636. https://doi.org/10.1007/s00024-019-02331-z.

Lyubushin, A., 2020c. Global Seismic Noise Entropy. Front. Earth Sci. 8611663. https://doi.org/10.3389/feart.2020.611663.

Lyubushin, A., 2021a. (2021a) Global Seismic Noise Wavelet-based Measure of Nonstationarity. Pure Appl. Geophys. 178, 3397–3413. https://doi.org/10.1007/s00024-021-02850-8.

Lyubushin, A., 2021b. Low-frequency seismic noise properties in the Japanese islands. Entropy 2021 (23), 474. https://doi.org/10.3390/e23040474.

Lyubushin, A., 2022. Investigation of the Global Seismic Noise Properties in Connection to Strong Earthquakes // Front. Earth Sci. 10905663. https://doi.org/10.3389/feart.2022.905663.

Lyubushin, A., 2023. Spatial correlations of global seismic noise properties. Appl. Sci. 13 (12), 6958. https://doi.org/10.3390/app13126958.

Lyubushin A. (2018) Synchronization of Geophysical Fields Fluctuations. Tamaz Chelidze, Luciano Telesca, Filippos Vallianatos (eds.), Complexity of Seismic Time Series: Measurement and Applications, Elsevier 2018, Amsterdam, Oxford, Cambridge. Chapter 6. P.161-197. DOI: https://doi.org/10.1016/B978-0-12-813138-1.00006-7.

Mallat, S.A., 1999. Wavelet tour of signal processing, Second ed. Academic Press, San Diego, London, Boston, New York, Sydney, Tokyo, Toronto.

Marple, S.L., 1987. Digital spectral analysis with applications. Prentice-Hall Inc., Englewood Cliffs, New Jersey.

Matzka, J., Chulliat, A., Mandea, M., Finlay, C.C., Qamili, E., 2010. Geomagnetic observations for main field studies: from ground to space. Space Sci. Rev. 155, 29–64. https://doi.org/10.1007/s11214-010-9693-4.

Press, W.H., Flannery, B.P., Teukolsky, S.A., Vettering, W.T., 1996. Numerical Recipes. second ed., Chapter 13, Wavelet Transforms, Cambridge Univ. Press, Cambridge.

Rabeh, T., Miranda, M., Hvozdara, M., 2010. Strong earthquakes associated with high amplitude daily geomagnetic variations. Nat. Hazards 53, 561–574. https://doi.org/10.1007/s11069-009-9449-1.

Rao, C.R., 1965. Linear statistical inference and its applications. John Wiley & Sons, Inc. N.Y, London, Sydney.

Sarkar, S., Gwal, A.K., Parrot, M., 2007. Ionospheric variations observed by the DEMETER satellite in the mid-latitude region during strong earthquakes. J. Atmos. Sol. Terr. Phys. 69, 1524–1540. https://doi.org/10.1016/j.jastp.2007.06.006.

Sarlis N.V., Christopoulos S.-R. G., Skordas E.S. (2015) Minima of the fluctuations of the order parameter of global seismicity, Chaos, 2015, 25:063110(9). https://doi.org/10.1063/1.4922300.

Serita, A., Hattori, K., Yoshino, C., Hayakawa, M., Isezaki, N., 2005. Principal component analysis and singular spectrum analysis of ULF geomagnetic data associated with earthquakes. Nat. Hazards Earth Syst. Sci. 5, 685–689. https://doi.org/10.5194/nhess-5-685-2005.

Shanker, D., Kapur, N., Singh, V., 2001. On the spatio temporal distribution of global seismicity and rotation of the Earth - a review. Acta Geod. Geoph. Hung. 36, 175–187. https://doi.org/10.1556/AGeod.36.2001.2.5.

Thomas, J.N., Love, J.J., Johnston, M.J., 2009. On the reported magnetic precursor of the 1989 Loma Prieta earthquake. Phys. Earth Planet. In. 173, 207–215. https://doi.org/10.1016/j.pepi.2008.11.014.

Varotsos P.A., Sarlis N.V., and Skordas E.S. (2003) Electric fields that "Arrive" before the time derivative of the magnetic field prior to major earthquakes, Physical Review Letters, 2003, 91:148501(4). https://doi.org/10.1103/PhysRevLett.91.148501.

Varotsos, P.A., Sarlis, N.V., Skordas, E.S., 2024. Direct interconnection of seismicity with variations of the Earth's electric and magnetic field

before major earthquakes. Europhys. Lett. 146, 22001. https://doi.org/10.1209/0295-5075/ad37d6.

Vogel, M.A., Wong, A.K.C., 1979. PFS clustering method. IEEE Trans. Pattern Anal. Mach. Intell 1 (3), 237–245 https://pubmed.ncbi.nlm.nih.gov/21868854/. https://doi.org/10.1109/tpami.1979.4766919.

Xu, G.; Han, P.; Huang, Q.; Hattori, K.; Febriani, F.; Yamaguchi, H. (2013) Anomalous behaviors of geomagnetic diurnal variations prior to the 2011 off the Pacific coast of Tohoku earthquake (Mw9.0). J. Asian Earth Sci. 2013, 77, 59–65. https://doi.org/10.1016/j.jseaes.2013.08.011.